Supplement of Biogeosciences, 17, 793–812, 2020
https://doi.org/10.5194/bg-17-793-2020-supplement

Biogeosciences Open Access EGU

Supplement of

Diel quenching of Southern Ocean phytoplankton fluorescence is related to iron limitation

Christina Schallenberg et al.

Correspondence to: Christina Schallenberg (christina.schallenberg@utas.edu.au)

Supplementary Information:

- Figures S1-S16
- Comparison of conditions underlying measurements of primary productivity
- Treatment and calibration of ac-9 data (including Figures S12-S16 and Table S1)

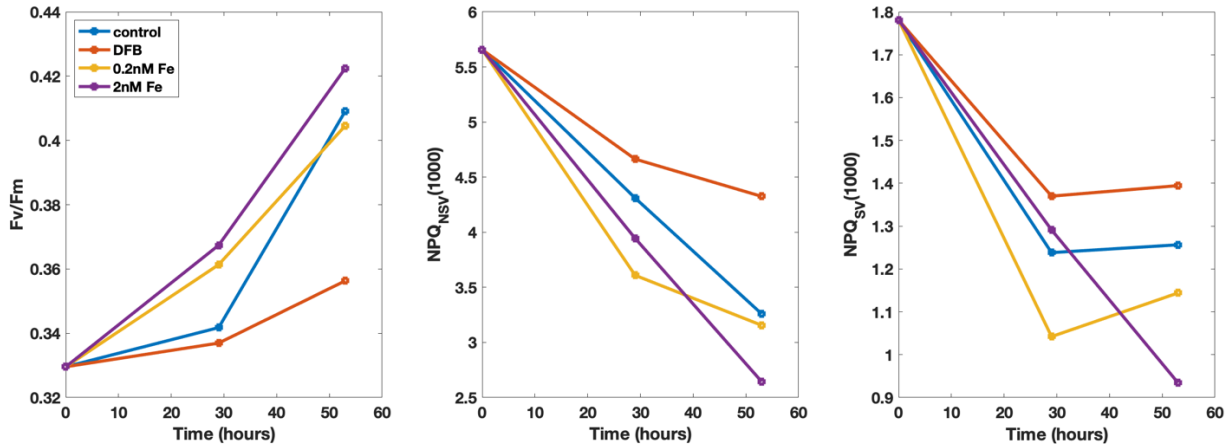

Figure S1: Time course of Fv/Fm as well as the two NPQ parameters for incubation 1, showing the results at the end point (after 52 h) as well as at 29 h. Colors represent different treatments as indicated in the figure legend. It is evident that the changes observed at 52 h were already underway at 29 h, but were generally more pronounced after 52 h.

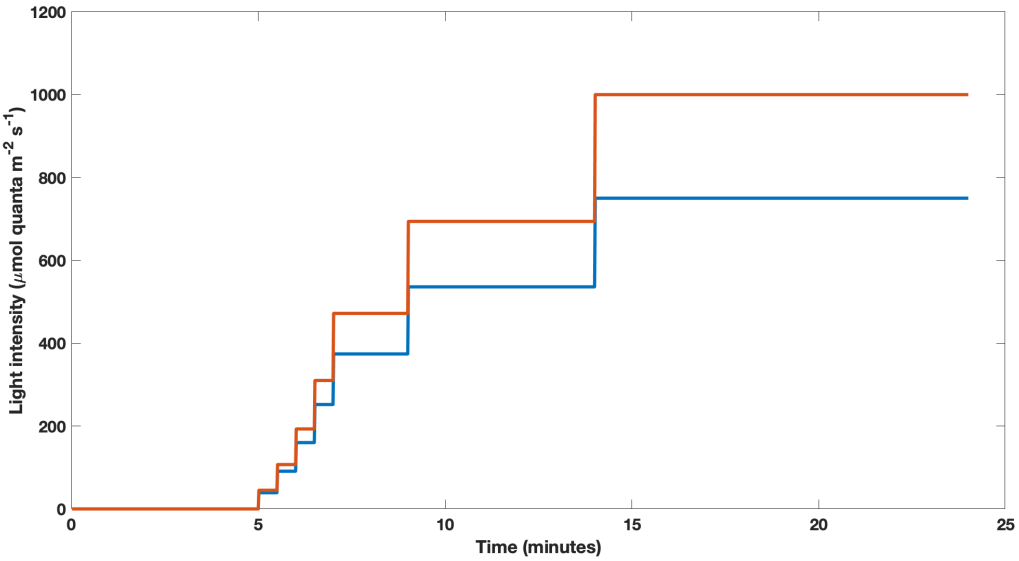

Figure S2: Schematic of time steps and light levels in fluorescence light curves employed in this study. The blue line relates to underway samples (with maximum light level of 750 µmol quanta m^{-2} s^{-1}) and the red line refers to samples from the deckboard incubation with maximum light levels of 1000 µmol quanta m^{-2} s^{-1}. The different maximum light intensities were chosen such that maximum NPQ was achieved for each set of samples, while still providing an induction curve in the FRRf that could be readily fit to the expected functionality (at higher light intensities the curve becomes too flat to achieve a good fit). Phytoplankton in the incubations displayed variable fluorescence at higher light intensities than phytoplankton in the underway samples, most likely due to high-light acclimation in the incubated samples.

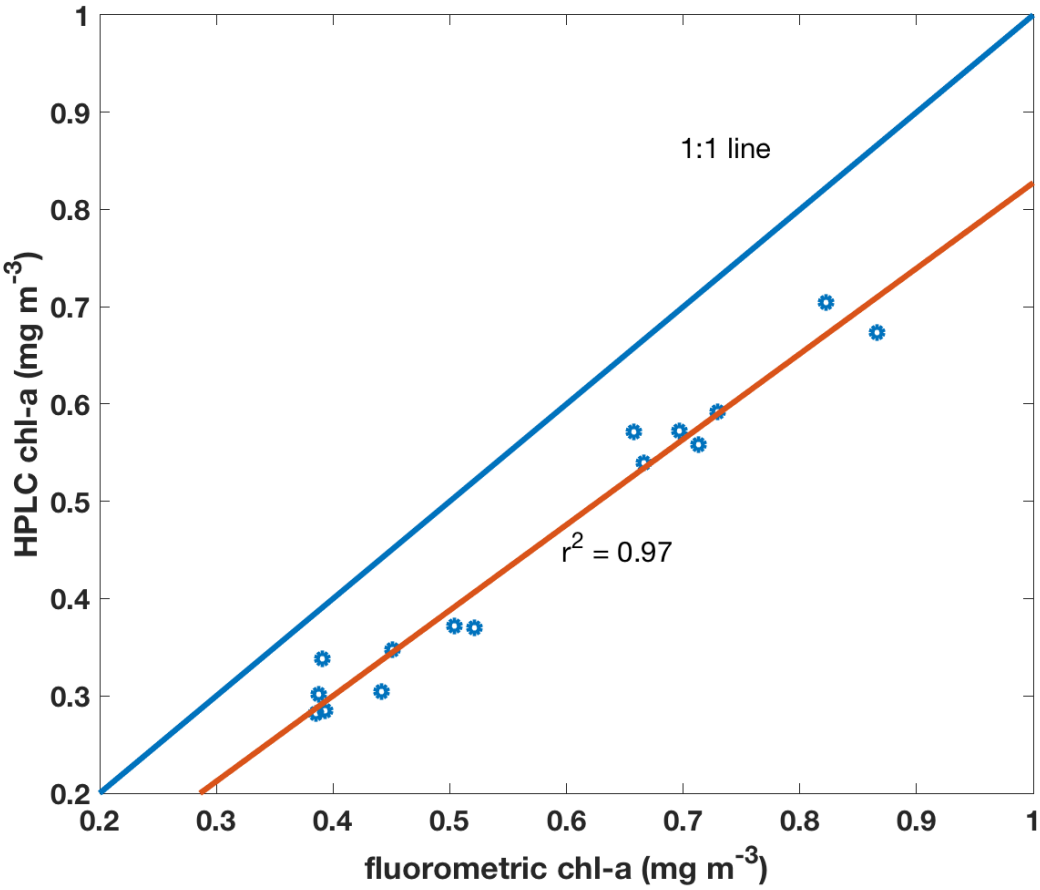

Figure S3: Comparison of Chl-a estimates from fluorometric analyses and HPLC. Linear regression yields the following expression: $Chl_{HPLC} = Chl_F * 0.879 - 0.052$ ($r^2 = 0.97$, n = 15, standard error of the estimate = 0.029 mg m^{-3}).

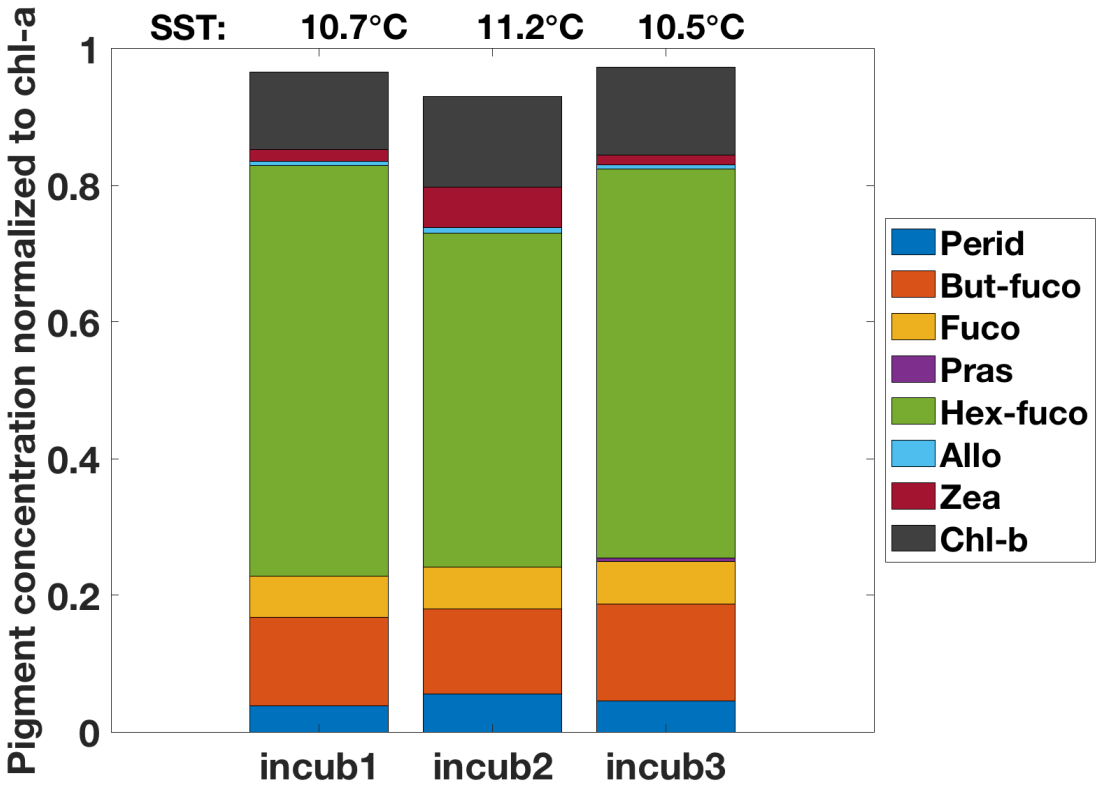

Figure S4: Initial pigment concentrations relative to Chl-a from HPLC analyses for the three incubation experiments. The sea surface temperature at time of sampling is indicated at the top. The HPLC analyses indicate that the sampled waters were dominated by haptophytes. Some diatoms and chrysophytes may also have been present.

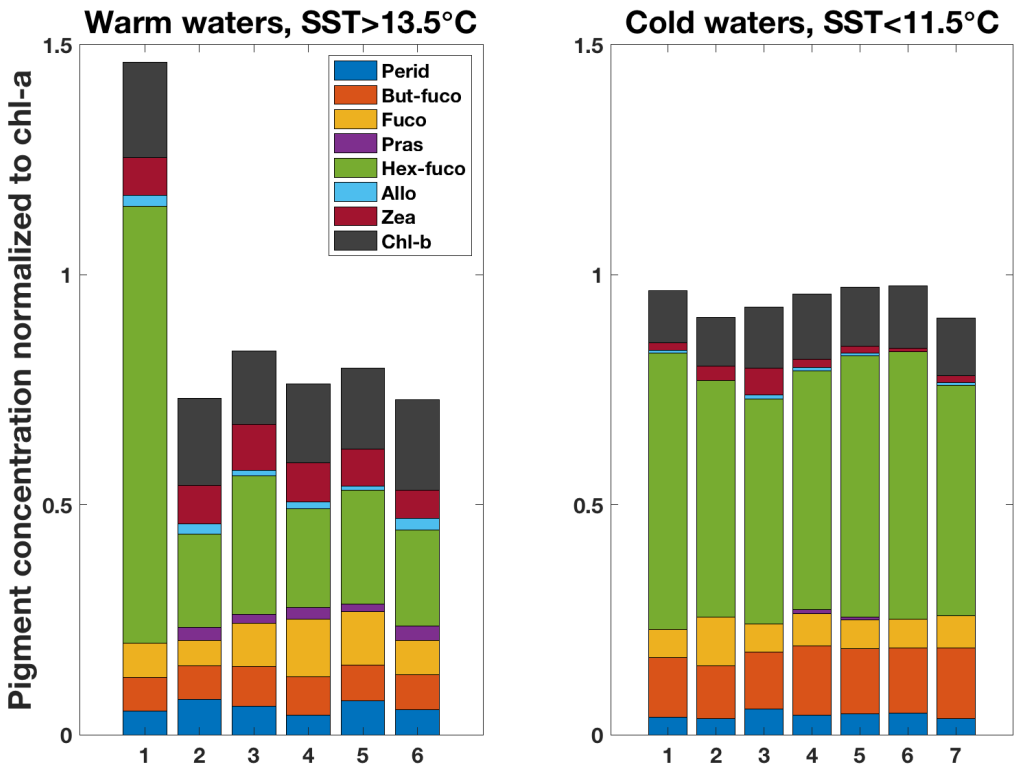

Figure S5: Pigment concentrations relative to Chl-a from HPLC analyses of underway samples, grouped by SST. The HPLC analyses indicate that the cold waters were dominated by haptophytes, and some diatoms and chrysophytes may also have been present. Haptophytes, as indicated by the presence of Hex-fuco, were also present in the warm water mass, but they were less dominant here than in the cold waters. The warm waters also hosted some green algae (prasinophytes) and likely some diatoms, and some cyanobacteria may have been present, most likely *Synechococcus*. The data suggest that both the warm and cold waters had mostly similar phytoplankton sizes, except for the possibility of *Synechococcus* in the warm waters.

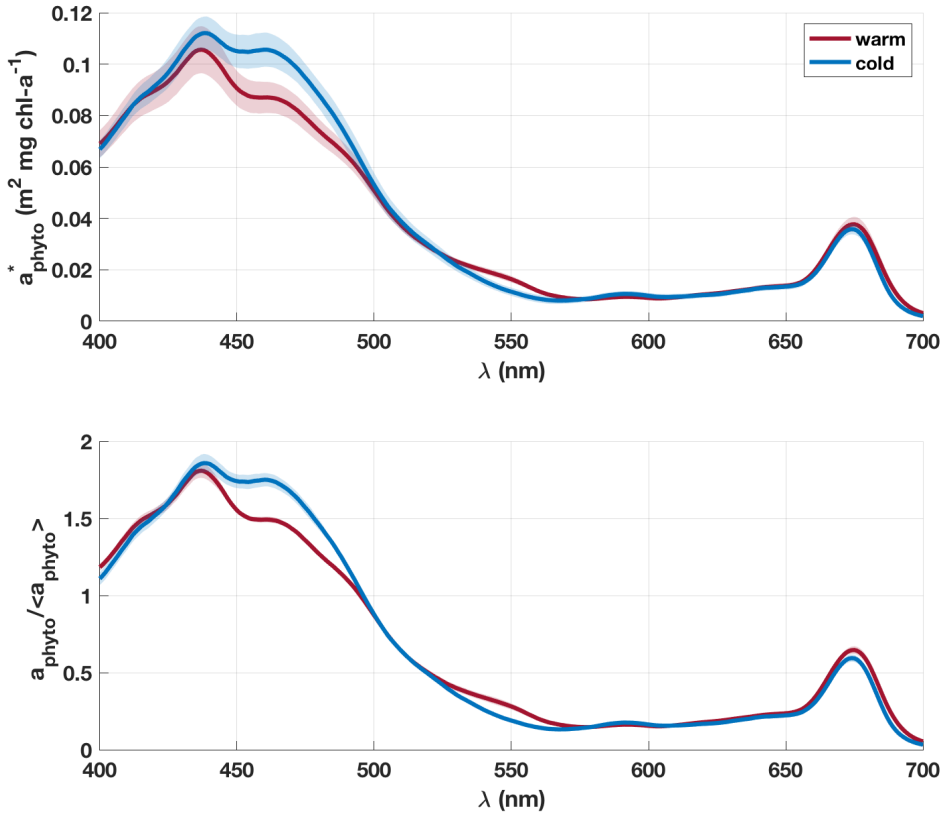

Figure S6: Mean phytoplankton absorption spectra for the respective water masses (red = warm; blue =cold) from underway samples (n=17), with one standard deviation indicated by shaded areas. Top panel shows phytoplankton absorption spectra normalized to the respective Chl-a concentrations, while the bottom panel shows phytoplankton absorption spectra normalized to the mean absorption $<a_{phyto}>$.

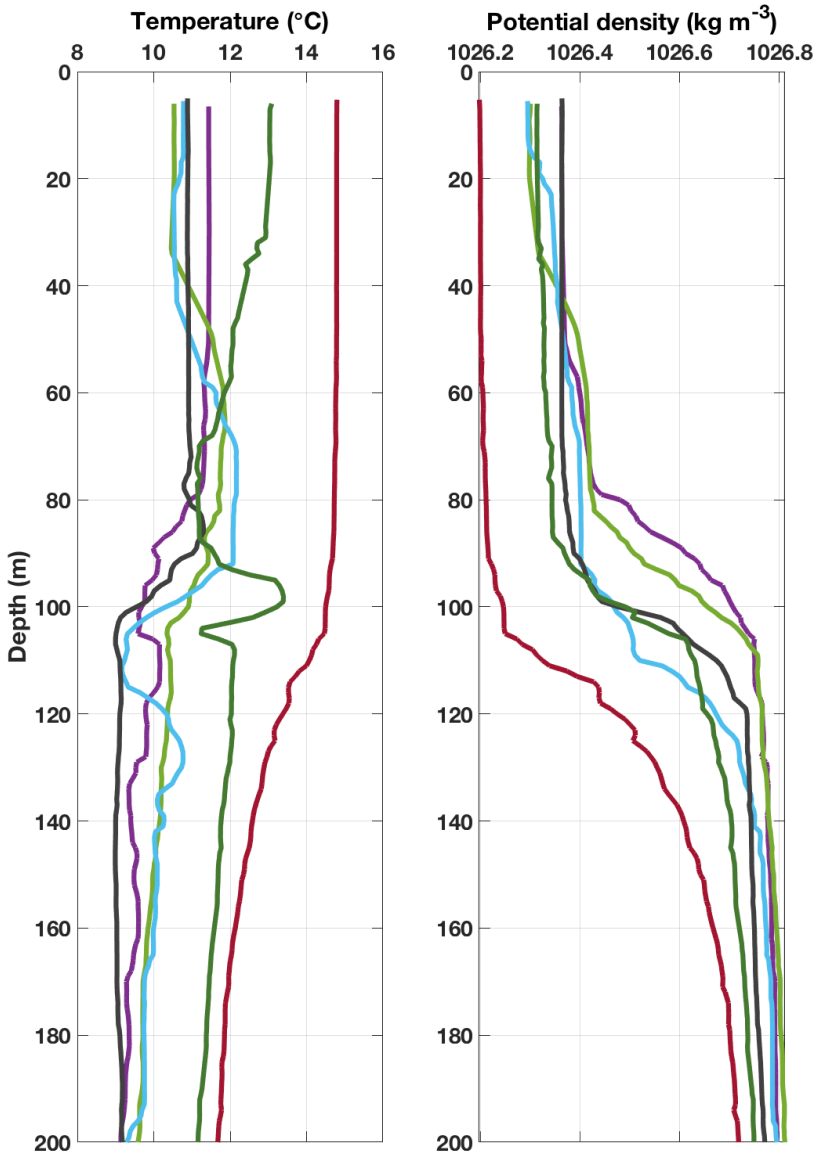

Figure S7: Temperature and density profiles from CTD casts on the SOTS voyage in 2018. The red line is the only profile from the warm water mass (SST>13.5°C), and the dark green profile was likely measured in a transitional zone. All other profiles are from the cold water mass and show varying mixed layer depths.

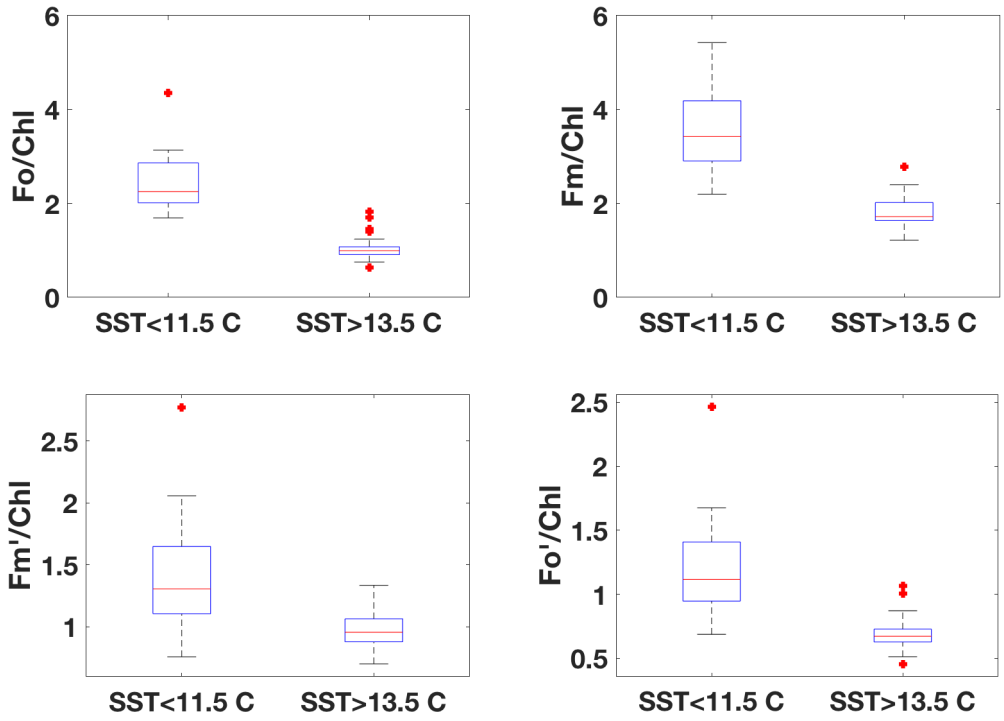

Figure S8: Individual fluorescence parameters measured with the FRRf on underway samples, normalized to Chl-a and grouped by SST. The minimum and maximum fluorescence in the dark-adapted state (F_o and F_m) are shown in the top panels, while the respective measurements in the light-acclimated state (in this case at 750 µmol quanta m^{-2} s^{-1}) are shown at the bottom. All parameters are significantly different ($p<<0.01$) between the two water masses.

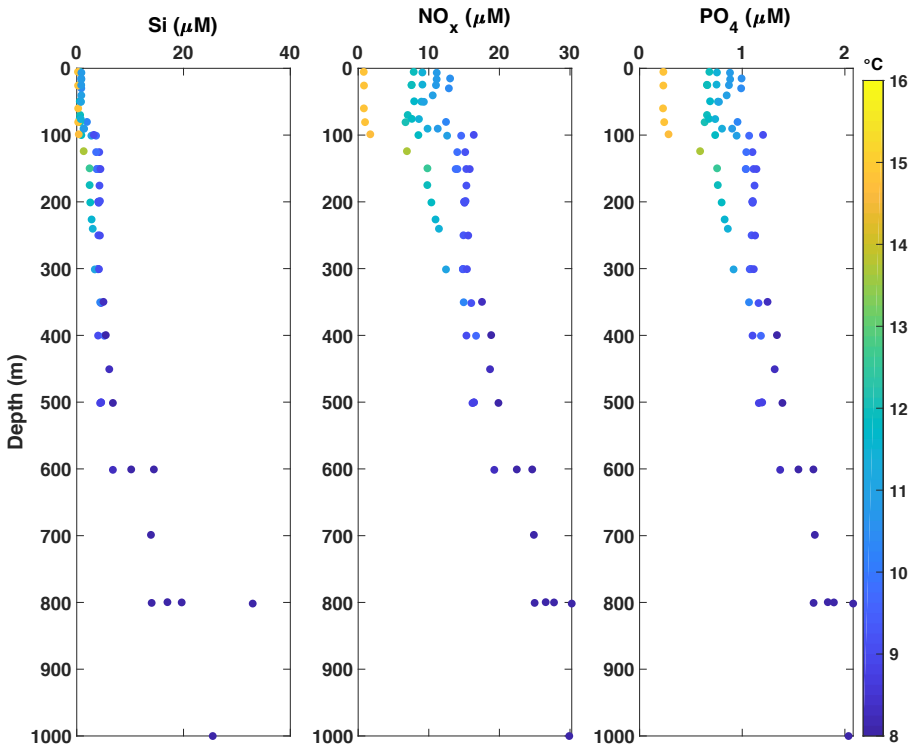

Figure S9: Profiles of macronutrient concentrations measured on the SOTS voyage in 2018, colour-coded by the respective temperature. Only one profile was measured in the warm water mass (yellow colours at the surface), exhibiting significantly lower NO_x and PO_4 concentrations than the colder water mass.

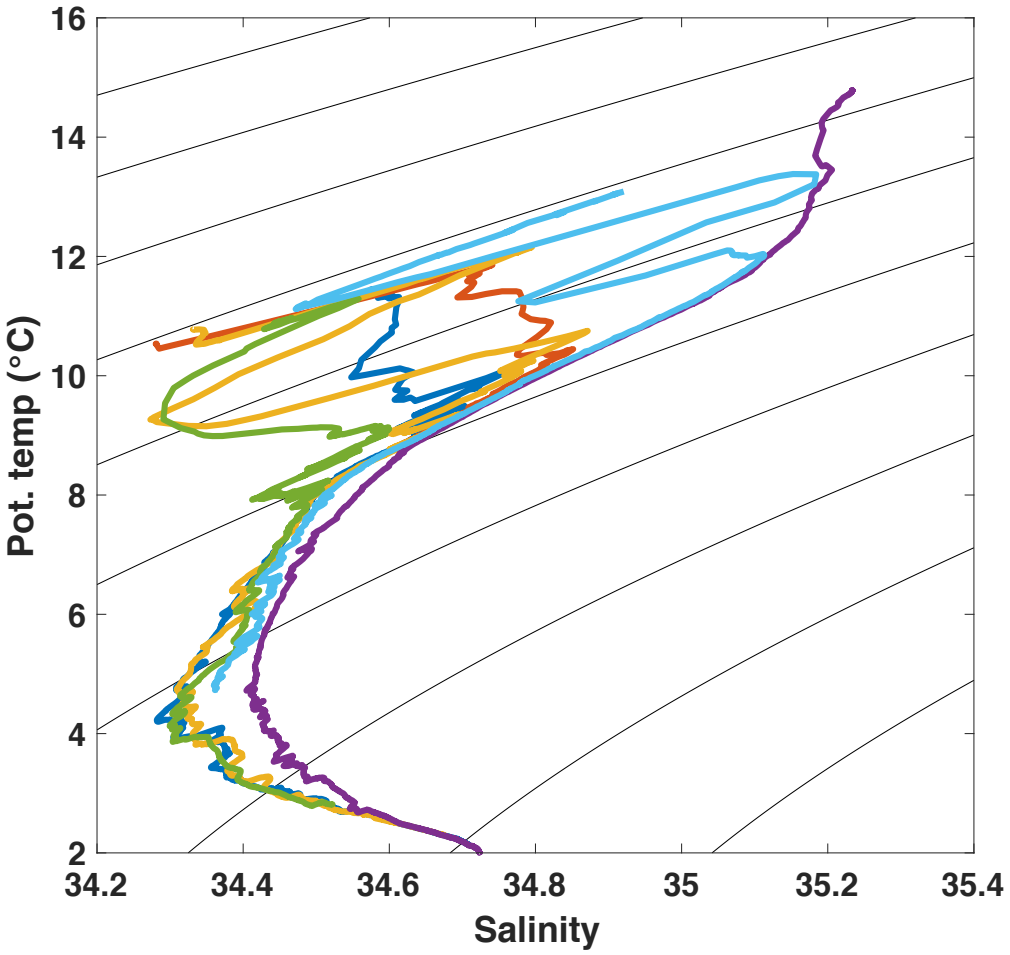

Figure S10: Temperature-salinity diagram for CTD data from the SOTS 2018 voyage. The purple line indicates data from the water mass with a warmer SST signature. This water mass also exhibited a saltier salinity minimum at depth, consistent with this water mass originating further north than the Subantarctic cold water mass (Herraiz-Borreguero & Rintoul, 2011).

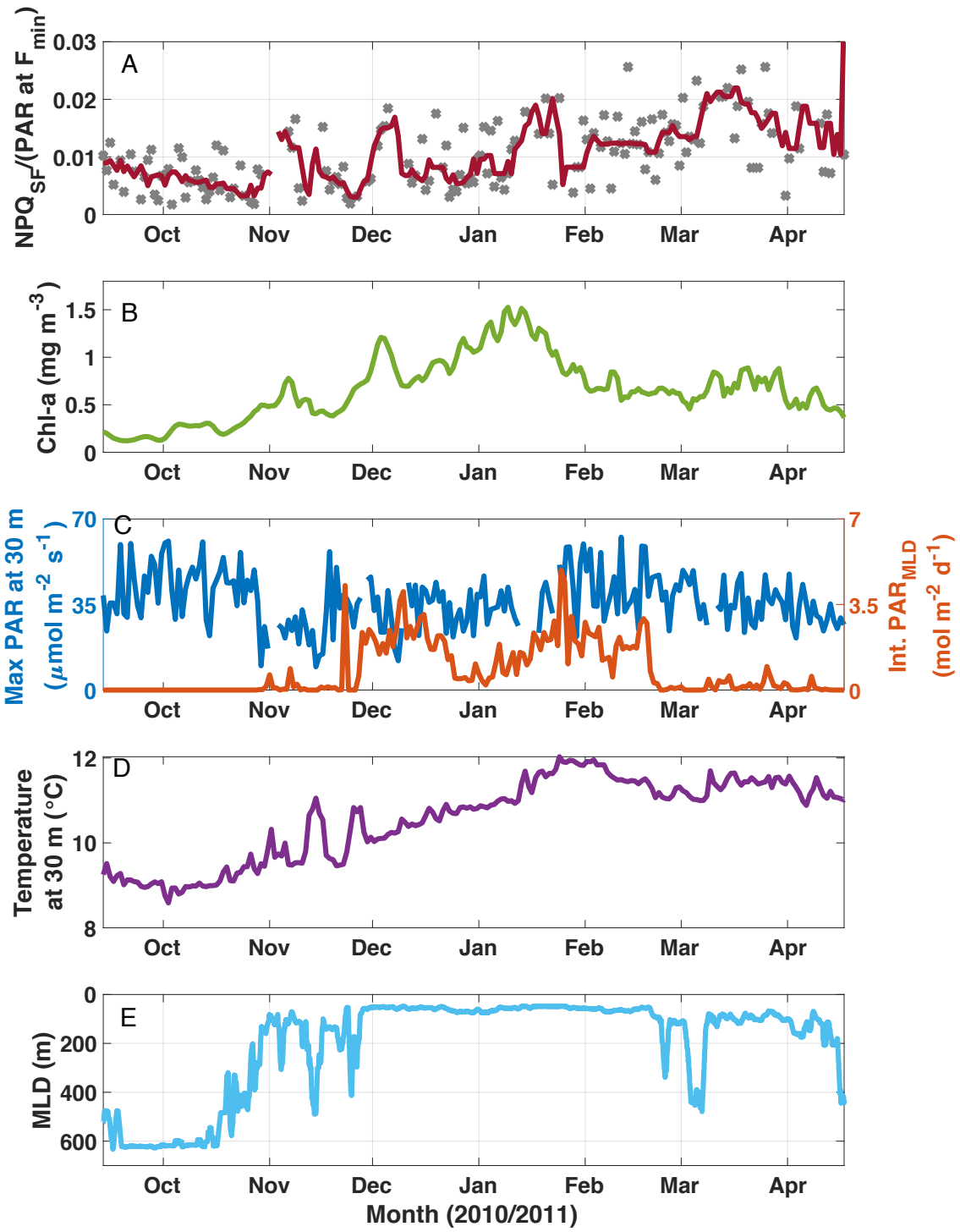

Figure S11: SOTS mooring data for October 2010 to April 2011; same as Figure 9 in the main manuscript except for panel A. Here, panel A shows NPQ_{SF} normalized to PAR at F_{min}, with grey markers indicating daily estimates and the red line a 7-day running median. Panel B shows a 3-point running mean over daily Chl-a concentrations estimated based on calibrated fluorescence; panel C shows maximum PAR recorded at 30 m for any given day (left axis) and the integrated daily PAR for the mixed layer (right axis). Water temperature at 30 m is shown in panel D, and the mixed layer depth is indicated in panel E.

Comparison of conditions underlying measurements of primary productivity:

Our discussion in Section 3.2.4 compares findings regarding primary productivity between our study and that of Westwood et al. (2011). A number of factors can contribute to the observed differences in primary productivity, hence we compare the conditions found in the two studies in order to pinpoint the most likely candidate. Sea surface temperatures were similar between Westwood et al. (2011) and our study (12°C vs 11°C, respectively), mixed layer depths were also similar (mean=38 +/- 11 m and mean=35 +/- 1 m, respectively), but the column-integrated Chl-a was different: mean=46 +/- 11 mg m^{-2} vs mean=13 mg m^{-2}. However, the fact that biomass was lower in our study could also be the result of lower iron concentrations (and lower rates of primary productivity). Moreover, normalizing the mean column-integrated primary productivity for each study by the mean column-integrated Chl-a concentration yields 85 mg C (mg Chl)$^{-1}$ d^{-1} for Westwood et al. (2011) and 31 mg C (mg Chl)$^{-1}$ d^{-1} for our study, indicating that the Chl-normalized primary productivity was lower during our study (in Austral fall) than in the Westwood et al. study in Austral summer. The conclusion that primary productivity was lower in our study thus holds, with Fe limitation a probable cause, as discussed in Section 3.2.4.

Treatment and calibration of ac-9 data:

The largest problem encountered on the cruise was the presence of bubbles in the flow tubes, as has been reported previously (Slade et al., 2010). This problem was intermittent, i.e. there were whole multi-hour stretches without bubbles, but overall the problem persisted through the duration of the cruise. In order to make the most of the data, the raw data (file by file and wavelength by wavelength, both filtered and unfiltered) were processed as follows:

1) A moving standard deviation for 1 minute of data (359 data points) was calculated for each file, and at the end the median of that standard deviation was calculated (stdev).
2) A running median (1-minute, i.e. 359 data points) was then calculated, and any raw values that fell outside the envelope defined by the median +/-3*stdev were flagged as bubbles and removed from further processing.
3) A running median was calculated of the remaining data over a 999-point window (<3 minutes), and these smoothed data were binned into 1-minute medians.
4) The filtered data were interpolated based on the corresponding time stamps to match the unfiltered data and were then subtracted from the unfiltered data, yielding particulate absorption (a_p). This step, in principle, accounts for issues relating to absolute calibration of the absorption channels such as dependence on the clean water offset as well as temperature and salinity corrections (e.g., Slade et al. 2010). However, in practice there will still be temperature offsets (i.e., the filtered and unfiltered measurements cannot be expected to have been at the exact same temperatures), and there is also an over-estimation of absorption in reflective flow tubes that should be accounted for with a scattering correction (Slade et al. 2010). The limited wavelengths of the ac-9 make a comprehensive temperature and scattering correction – such as is recommended for hyperspectral instruments – impossible. We thus opted to not apply any further corrections, noting that the expected uncertainty due to this omission is ~$0.006\Delta T$ at λ=412 nm, and less at longer wavelengths (Slade et al. 2010).
5) Particulate absorption line height at 676 nm (LH(676), m^{-1}) was then calculated following Roesler and Barnard (2013), subtracting a baseline based on absorption measurements at 650 and 715 nm.
6) Before calibrating the ac-9 data against discrete Chl-a and phytoplankton absorption measurements from filter pad, the LH(676) time series was further smoothed with a 1-hour running median to reduce residual noise. This step considerably improved calibrations for both Chl-a and mean phytoplankton absorption $<a_{phyto}>$ (see Figures and Table below).

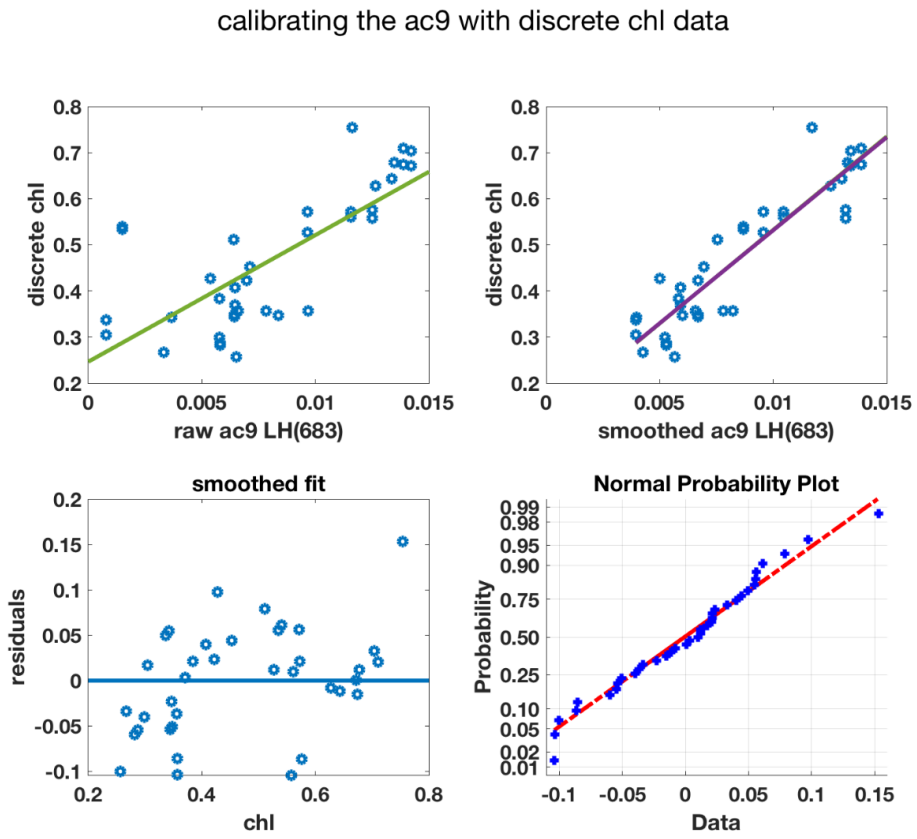

Figure S12: Calibration of ac-9 line height (LH(676)) against discrete Chl-a (HPLC and fluorometric samples combined). Top panels: Calibrations for raw (left) and smoothed (right) ac-9 data (1-hr running median), with regression lines indicated in green and purple. Bottom: Residuals of the regression with smoothed ac-9 data as a function of Chl-a, and normal probability plot of the same residuals. See Table S1 for statistics and calibration coefficients.

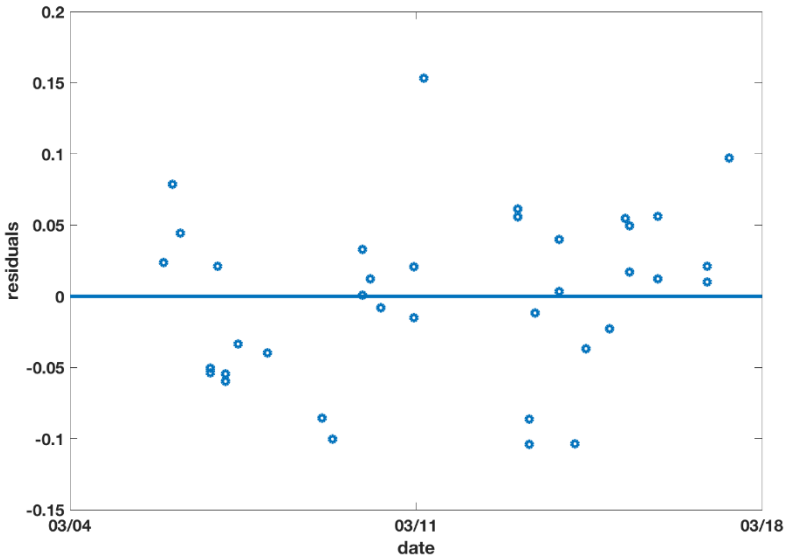

Figure S13: Residuals of the smoothed calibration of ac-9 line height (LH(676)) against discrete Chl-a (see above) as a function of time, showing no evidence of bio-fouling.

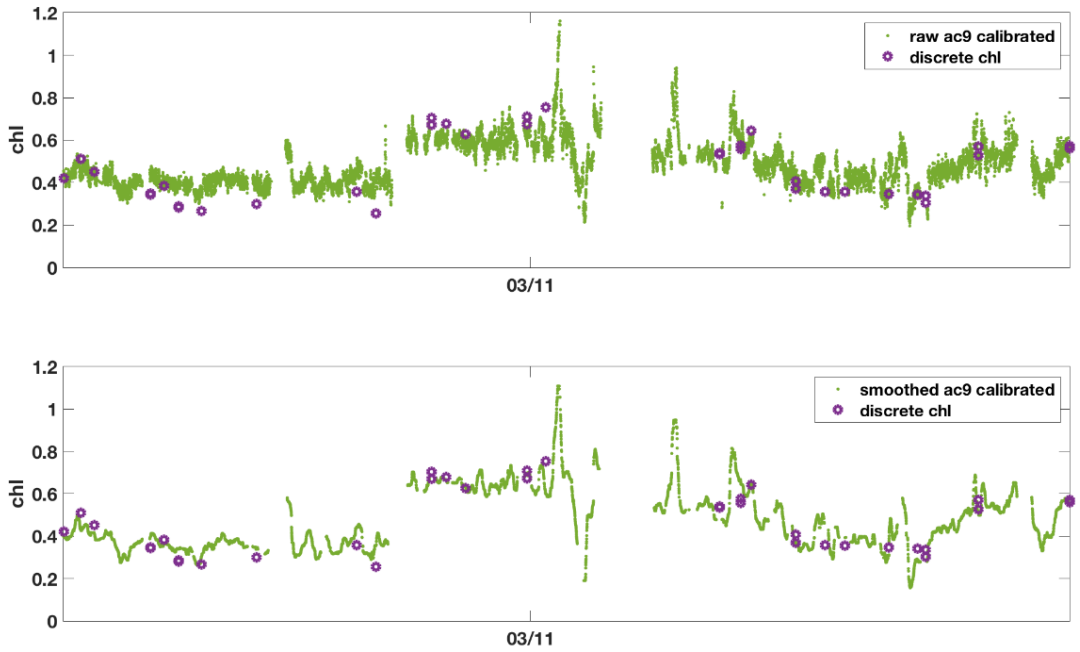

Figure S14: Calibrated ac-9 data (green) overlain with discrete Chl-a samples (purple). ac-9 data calibrated as indicated in Figure S10 and Table S1, i.e. using the raw and smoothed ac-9 data respectively. Top panel shows the raw ac-9 data and bottom-panel shows the smoothed ac-9 data (1-hr running median). It is evident that the smoothing improves the match-ups.

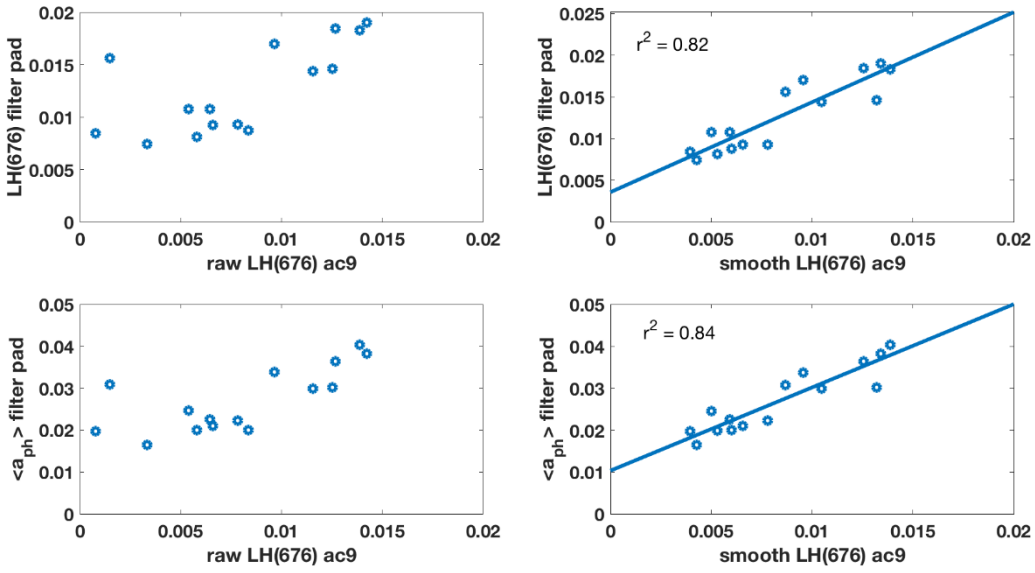

Figure S15: Relationship between raw (left) and smoothed (right) ac-9 LH(676) and phytoplankton absorption measurements from filter pad analyses. Top panels show relationships to LH(676) from filter pad absorption, bottom panels show relationships with mean phytoplankton absorption $<a_{ph}>$ from filter pads. Linear regression lines only shown for smoothed ac-9 data.

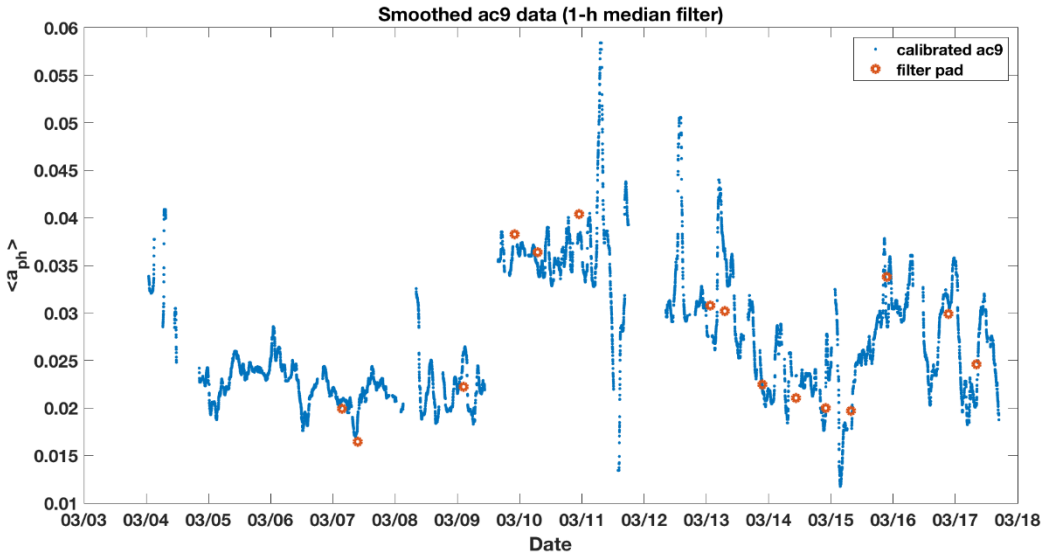

Figure S16: Calibrated ac-9 time series (smoothed with a 1-hr running median) of mean absorption $\langle a_{ph} \rangle$ in blue, with discrete filter pad measurements of $\langle a_{ph} \rangle$ overlain in red.

Table S1. Statistics of the respective ac-9 calibrations:

LH(676) ac-9 against:	**r^2 raw**	**SEE raw**	**Slope raw**	**Intercept raw**	**r^2 smoothed**	**SEE smoothed**	**Slope smooth**	**Intercept smoothed**
Chl-a	0.56	0.15	27.47	0.246	0.84	0.07	40.56	0.127
LH(676) filter pad	0.48	0.004	0.68	0.007	0.82	0.002	1.08	0.004
$\langle a_{ph} \rangle$ filter pad	0.54	0.009	1.30	0.017	0.84	0.005	1.99	0.010

SEE = standard error of the estimate

References

Herraiz-Borreguero, L., and Rintoul, S. R.: Regional circulation and its impact on upper ocean variability south of Tasmania. Deep-Sea Res. Pt. II, 58(21–22), 2071–2081, https://doi.org/10.1016/j.dsr2.2011.05.022, 2011.

Roesler, C. S., and Barnard, A. H.: Optical proxy for phytoplankton biomass in the absence of photophysiology: Rethinking the absorption line height. Methods in Oceanography, 7, 79–94, https://doi.org/10.1016/j.mio.2013.12.003, 2013.

Slade, W., Boss, E., Dall'Olmo, G., Langner, M., Loftin, J., Behrenfeld, M., … Westberry, T.: Underway and moored methods for improving accuracy in measurement of spectral particulate absorption and attenuation. J. Atmos. Oceanic Tech., 27, 1733–1746, https://doi.org/10.1175/2010JTECHO755.1, 2010.

Westwood, K. J., Griffiths, F. B., Webb, J. P., and Wright, S. W.: Primary production in the Sub-Antarctic and Polar Frontal Zones south of Tasmania, Australia; SAZ-Sense survey, 2007. Deep-Sea Res. Pt. II, 58, 2162–2178, 2011.